Journal of Directed Energy, **1**, Spring 2004, 111–129

Q^* and In Situ Measurements of Temperatures on the Surfaces of Samples Irradiated by a Sequence of Picosecond Laser Pulses

J. Grun*
Plasma Physics Division, Naval Research Laboratory, Washington, D.C. 20375

C. K. Manka
Research Support Instruments, Lanham, Maryland 20706

R. Fischer
Plasma Physics Division, Naval Research Laboratory, Washington, D.C. 20375

R. F. Wenzel
Material Science and Technology Division, Naval Research Laboratory, Washington, D.C. 20375

R. Cozzens
Chemistry Division, Naval Research Laboratory, Washington, D.C. 20375

and

M. Shinn
Jefferson Laboratory, Newport News, Virginia 23606

One-inch-diameter samples of various materials, such as stainless steel, painted and unpainted aluminum, fused silica, and fiberglass composites, were irradiated for several seconds, at pulse repetition rates of tens of megahertz, by a sequence of picosecond-duration pulses from a free-electron laser operating at a wavelength of 3.1 μm. In a typical experiment the laser irradiated a few-millimeter-diameter spot with a number of kilojoules, resulting in kilowatt-per-square-centimeter average irradiances and substantially higher peak irradiances. These experiments were the first to examine the lethality, measured as Q^* (laser energy in kilojoules required for removing 1g of material), of a long sequence of picosecond-duration laser pulses in an irradiance regime relevant to high energy laser lethality, i.e., utilizing laser intensities that have a chance of propagating a significant distance in the atmosphere without much loss of energy. In situ diagnostics were used to measure space- and time-resolved temperature profiles on the laser-irradiated and backsides of the samples. Heating and cooling of the samples,

Received January 30, 2003; revision received April 12, 2003.
*Corresponding author; e-mail: grun@nrl.navy.mil.

melting, boiling, hole burning, flow of liquid matter, and breakup of composites were measured. Results of these experiments and a comparison to postshot analysis of the samples are presented.

KEYWORDS: Free electron, Laser, Lethality, Picosecond, Q^*, Temperature

1. Introduction

During June and September 2001 we examined the vulnerability of various materials to irradiation by a several-second sequence of picosecond-duration pulses from a free-electron laser (FEL) at average irradiances of 0.5–10 kW/cm^2 in a few-millimeter-diameter spot.[6] These experiments were the first to examine the material damage potential of a long sequence of picosecond-duration laser pulses in an irradiance regime relevant to high-energy-laser lethality (HELL), i.e., utilizing laser intensities that have a chance of propagating a significant distance in the atmosphere without much loss of energy. The laser used was the Jefferson Laboratory's FEL,[2] operating at a wavelength of 3.1 μm; pulse duration of 1 ps; average powers of 300, 600, and 1,000 W; and with pulse repetition rates of 18.71, 37.42, and 74.85 MHz. To prevent molten material from resolidifying in situ, leading to erroneous inferences of Q^* (laser energy in kilojoules required for removing 1 g of material), most irradiations were done with the sample in an uncharacterized airflow of about Mach 0.1 (90 mph) from a nozzle directed upward, roughly 30 deg from vertical, across its front face. A total of 594 samples were tested, among them samples of stainless steel, painted and unpainted aluminum, and a variety of materials used in radomes, such as glass-cloth composites, Pyroceram, and slipped-cast fused silica.

During these experiments two types of time- and space-resolved in situ diagnostics that measured the front and back surface emission temperatures of the irradiated samples were fielded. With these, heating and cooling of the samples, hole burning, and flow of liquid matter were observed. Temperature profiles on the laser-irradiated side of the noncomposite samples were found to be flat even though the targets were irradiated by a Gaussian-like laser profile, showing that a uniform temperature distribution on a sample can be obtained even with a nonflat laser beam. In regions of some samples temperatures near the boiling temperatures of the material were measured. Temperature profiles of fiberglass composite samples exhibited a range of temperatures indicative of different processes occurring in different parts of the composite: Regions of resin cook-off, sublimation of carbonized char, and decomposition of the fiber cloth were observed.

Simultaneously with the temperature measurements, Q^* measurements were obtained using two methods, penetration time and mass removal. On metallic samples that were penetrated by the laser, Q^* was inferred from the equation $Q^* = It/\rho d$, where I is the irradiance in kilowatts per square centimeter, d and ρ are, respectively, the sample thickness and density, and t is the time to penetrate the sample. Penetration time was measured with a diode viewing laser light that penetrated the sample and was reflected from a graphite slab beam dump placed behind the sample. For samples that were not penetrated, mostly the nonmetals, the sample was weighed before and after irradiation and Q^* inferred from Q^* = laser kilojoules/weight loss in grams.

Detailed measurements, such as these, can be used to validate predictive laser-matter interaction codes and provide a basis for increased confidence (or reduced confidence) for the extrapolation of the damage measurements to full-scale weapons scenarios.

2. In Situ Diagnostics

Two types of real-time, in situ temperature diagnostics were deployed: 1) two four-color video cameras, one observing the front (i.e., laser illuminated) and one the back (side away from laser beam) of the sample; and 2) a time-resolved spectrometer observing the front of the sample. The four-color video cameras are capable of measuring the emission temperature of the laser-heated spot on the target front as a function of space and time, emission temperature of the target rear as a function of space and time, heat conduction in the lateral and axial directions, disassembly of composite materials, mass flow at the target front or back, and melting, boiling, and vaporization processes. Time to burn through is easily observed and can be correlated with temperature profiles on the front, laser-illuminated side. The spectrometer measures spatially averaged, time-resolved emission gray-body spectra from the heated spot, from which the temperature of the spot is determined. Also, the spectrometer is used to verify the gray-body assumptions used by the deconvolution algorithms of the four-color imager. Sometimes, lines of laser beam harmonics and lines from the heated sample material are observed superimposed on the gray-body spectrum. If present, these lines are ignored in the temperature deconvolution algorithm.

2.1. Four-color camera

Each of the two four-color video cameras uses a photographic lens to collect and collimate light emitted by the target.[†] A triple-dichroic/single-mirror module is placed in the path of the collimated light[‡] to split the parallel light beam into four separate components, each containing a different part of the incident spectrum. The spectral content of each beam is further refined by placing a narrow bandpass filter in its path. The four filters in our case were centered at 700, 750, 800, and 850 nm with bandwidths of 20, 40, 40, and 40 nm, respectively. After filtering, each beam passes through a common imaging lens, forming four simultaneously acquired, spatially identical but spectrally different images of the light-emitting region on a single 1,034 × 779 pixel charge-coupled device (CCD) camera chip, each image occupying one quadrant of the CCD detector area. The four images are continuously read out of the CCD and stored on a computer disk at a rate of 7–10 frames/s (depending on computer overhead). The software running the camera has been customized for this FEL experiment to achieve the stated acquisition rate, allow immediate review of data after a test, and provide for semiautomatic analysis of data and for production of movie sequences.

The use of four spectrally filtered images is important for accurate determination of temperature. A temperature can be estimated, and often is, from one- or two-color pyrometers. To infer a temperature with these diagnostics, however, one must assume that a material's emissivity[§] is known a priori and that its value does not vary with wavelength or temperature. In reality, the emissivity of most materials is not constant and incorrect temperature measurements result if a constant emissivity is assumed.[3,8] The emissivity of metals, for example, changes with wavelength, temperature, and degree of oxidation. Glasses and plastics

[†]The front four-color camera is placed at 18 deg to the sample normal and 78 cm away. The rear camera at 15 deg to the sample normal and 78 cm away.

[‡]Placing mirrors and filters in the path of a parallel beam minimizes image distortion.

[§]Emissivity is the ratio of thermal emission of an object to the emission of an ideal black body at the same temperature.

are transparent or translucent in some wavelength regions, making measurements in those wavelength regions prone to large errors. Four spectrally filtered images allow one to construct an algorithm that determines the emissivity, and then, once emissivity is determined, temperature can be accurately calculated from the relative amplitudes of signals in each channel.[7]

Pre- and posttest calibrations were performed on both cameras. The calibrations included 1) image registration, i.e., the spatial relationship between the images on the CCD camera; 2) image magnification; and 3) background readings and their spatial variations. The end-to-end sensitivity with wavelength of each camera channel was determined by illuminating the front lens with a known amount of spectrally pure light (lamp light passed through a monochrometer) and recording it on the four-frame camera's CCD. The channel sensitivities were then inserted into the data deconvolution software.

An additional calibration was performed to cross check the reduction algorithm. For this calibration a tungsten ribbon lamp was heated to a known temperature in the range of 2,200–2,800 K by passing through it a measured amount of current.[¶,9,10] The hot ribbon was then photographed by the four-frame camera and its temperature calculated using the four-frame camera's deconvolution algorithm with the channels sensitivities measured earlier. Then the calculated temperature and the ribbon's actual temperature were compared for consistency. Results agreed to within 10%.

2.2. Spectrometer

Emitted light from a 3-mm-diameter spot on the front of the irradiated target was collected by a lens, imaged into a fused silica multimode fiber, and delivered to a spectrometer and its detector. The detector output was saved on a personal computer at a rate of one record/0.1 ms. The spectrometer used a 300-lines/mm grating and 50-μm slit, which provided spectral coverage from 500 to 1,000 nm with 1-nm resolution. The spectrometer's data acquisition software was specially modified for this experiment to allow rapid data acquisition. Special software was written, as well, to semiautomatically handle the large amount of data acquired, to convert the spectra to emission temperatures, and to produce a movie of the result. The temperature of the imaged spot was calculated from the continuum part of the spectrum** by fitting its shape to the shape of a gray-body curve, with temperature and the emissivity serving as free parameters.

The wavelength scale and wavelength sensitivity of the spectrometer was calibrated end to end, in situ, with Pen-Ray Oriel spectral calibration lamps and the tungsten ribbon lamp placed at the location of the sample. Wavelength calibration was obtained from the spectral-lamp lines and the system response as a function of wavelength from the known absolute emission of the tungsten lamp.

Figure 1a shows a typical result of the spectroscopy diagnostic. The data shown are from a sample illuminated with a 1,000-W FEL beam operating at 37.4 MHz and focused to produce 3 kW/cm^2 on the sample surface. Shown are representative spectra, gray-body fits to the spectra, and the temperature history that was derived from the gray-body fits. Shot-to-shot reproducibility of the temperature is typically $\pm$10%, as shown in Fig. 1b.

¶NRL tungsten ribbon lamp 6858. The relationship between the ribbon's temperature and current was determined by the National Bureau of Standards (now NIST).

**Any lines present in the spectrum are ignored. The lines, when present, correspond to the harmonics of the FEL beam.

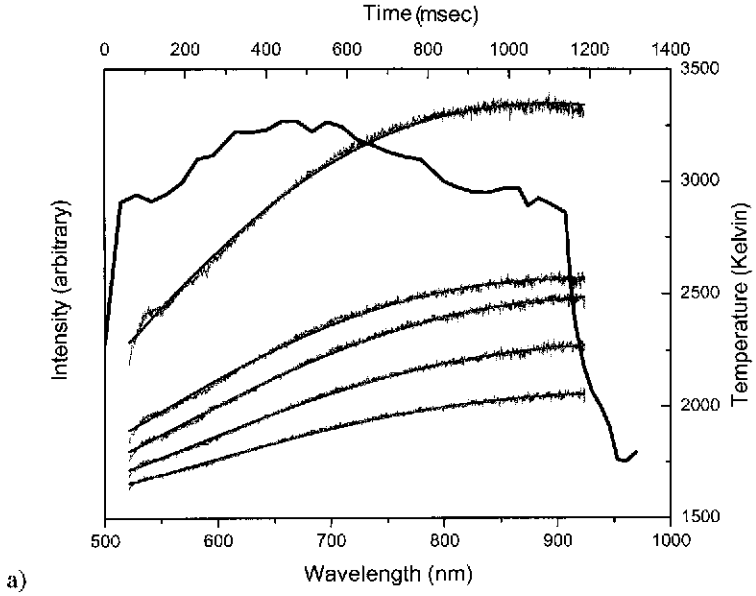

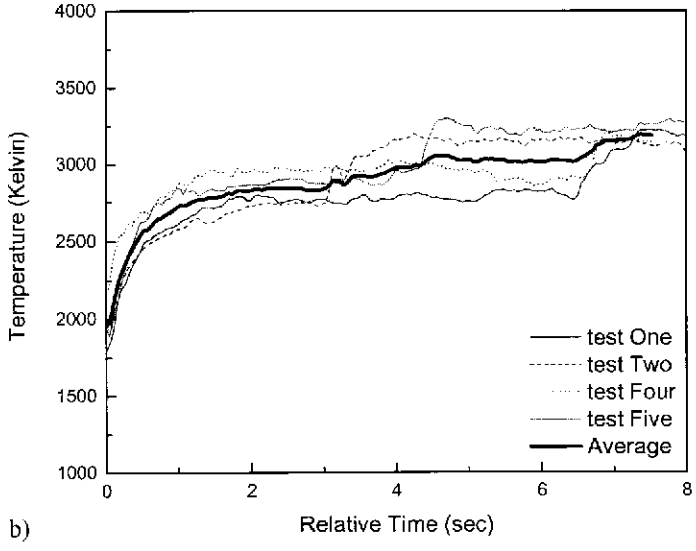

Fig. 1. a) How spectra are used to calculate temperature: Gray lines represent relative time sequences of spectra and gray-body fits to the spectra from a target illuminated with a 1,000-W FEL beam operating at 37.4 MHz and focused to produce 3 kW/cm^2 on the target surface. The spectra shown are corrected for detector dark current and detector sensitivity. From bottom to top the times shown are 39, 116, 268, 588, and 869 ms. The heavy black line is temperatures as a function of time derived from the gray-body fits. b) Shot-to-shot temperature reproducibility: Spectroscopically determined time histories of emission temperatures of a 3-mm-diameter spot on separate tests that used a 1-in.-diameter, 0.125-in.-thick stainless steel sample illuminated by a 600-W FEL beam running at 74.85 MHz and focused to 3 kW/cm^2. Individual temperature histories differ from their average by less than 10%.

3. Results

3.1. Stainless steel

Typical sequences of spatial temperature profiles on front surfaces of 304 stainless steel alloy are shown in Figs. 2 and 3. In Fig. 2, the sample was a 1-in.-diameter, 0.0625-in.-thick steel disk illuminated by a 300-W, 18.7-MHz FEL beam focused to 3 kW/cm^2 for 15 s. The first few frames do not show any image since the temperature of the sample is below the threshold of 800 K that can be measured by the camera in its current configuration.[††] By frame 5, arbitrarily designated to be 0 s, a small, 3-mm-diameter spot with a nearly uniform flattop temperature profile of about 1,500 K appears. The heated spot grows in diameter until, at 10 s, it reaches a diameter of 6 mm, still exhibiting a flat temperature profile of about 1500 K. Afterward the spot begins to shrink as the laser is turned off until it reaches 2.4-mm diameter at 13 s. Then the temperature again falls below the measurement threshold of the camera.

It is interesting to note that, although the incident laser beam has an approximately Gaussian shape, as measured by a time-integrating CCD camera, the resulting temperature profiles are mostly flat and show that a uniform temperature distribution on the sample can be obtained even with a nonuniform laser beam. This phenomenon is probably due to the temperature becoming clamped in the melting temperature range of 304 alloy stainless steel, which is (solidus to liquidus) 1,672–1,727 K.[‡‡,1]

Also visible in these pictures at times of 3.6–6.4 s is an asymmetry in the heated spot shape, a protrusion of mostly 1,500 K material at about 11 o'clock, which represents material flowing out of the heated spot under the influence of the estimated Mach 0.1 airflow.

Although the temperature profile is mostly flat, a thin region near the upper edge of the image tends to be much hotter, reaching temperatures of up to 3,000 K, as shown in the Fig. 2 graph. This temperature corresponds closely to 3,020 K, the textbook value for the boiling temperature of iron, the major constituent of steel.[5] Through most of the exposure, including the beginning, the hot region is just a sliver at the edge of the hot spot. Toward the end of the exposure, however, the hotter region occupies a more significant portion of the spot. At 13 s, as the spot is getting smaller due to the laser being shut off, roughly its upper half is hotter than 1,500 K.

It is quite possible that the presence of a hot upper lip and the presence of material flow in roughly the same direction are related. Suppose, for instance, that the molten material being pushed out of the heated spot by the airflow does not maintain good thermal contact with the cooler and now shadowed surface of the sample but that it is still being irradiated by the outer edges of the approximately Gaussian laser beam. Then the molten material would continue to absorb laser energy without being able to shed thermal energy via conduction into cooler parts of the metal. Enough energy could be trapped in this manner to raise the molten metal to liquid and then vaporization temperatures.

It is also possible to raise the sample temperature above its melting region by restricting heat flow from the entire sample or by heating it with more power than can be dissipated.

[††] The temperature threshold can be lowered by appropriate choice of narrow band filters and recording medium.

[‡‡] Alloys, being a mixture of elements, melt over a temperature range rather than at a single temperature. The heat of fusion is absorbed incrementally with temperature in a not-well-known manner. The solidus temperature is where the alloy first starts to melt (usually at grain boundaries where the minor constituents are concentrated). The liquidus temperature is where all the constituents of the metal are in a liquid mélange.

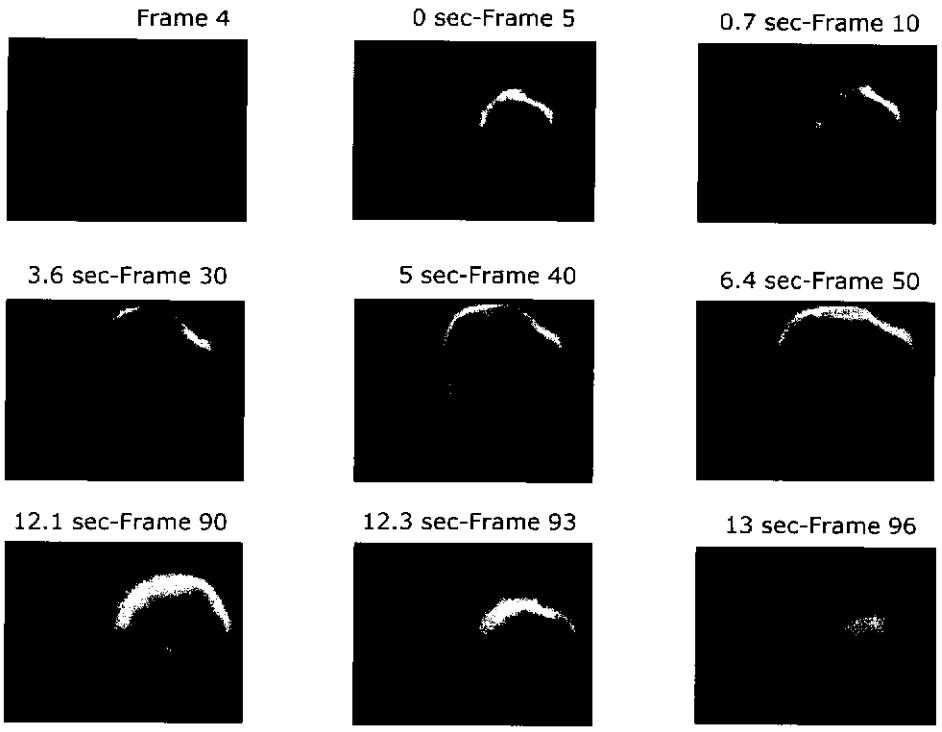

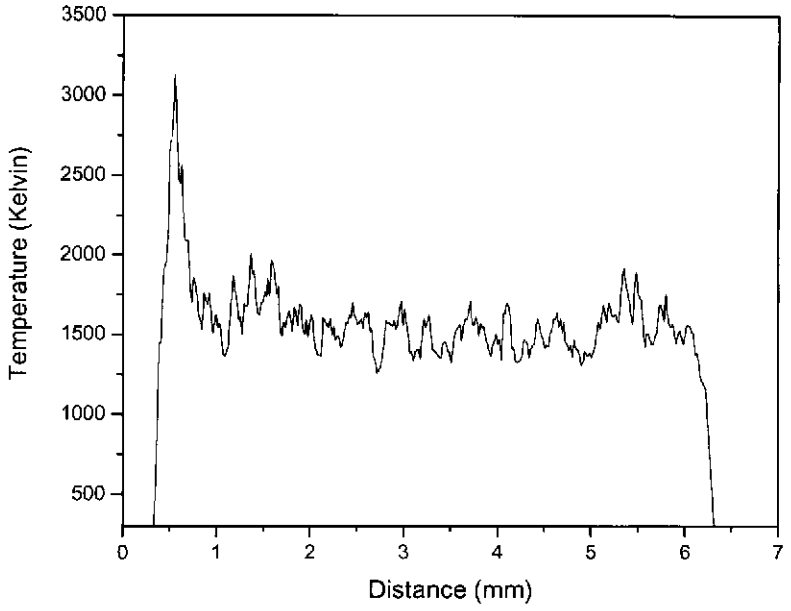

Fig. 2. Temperature profiles on the front surface of a 1-in.-diameter, 0.0625-in.-thick stainless steel disk illuminated by a 300-W, 18.7-MHz FEL beam focused to 3 kW/cm^2 for 15 s. The graph shows a representative lineout of temperature at 10 s.

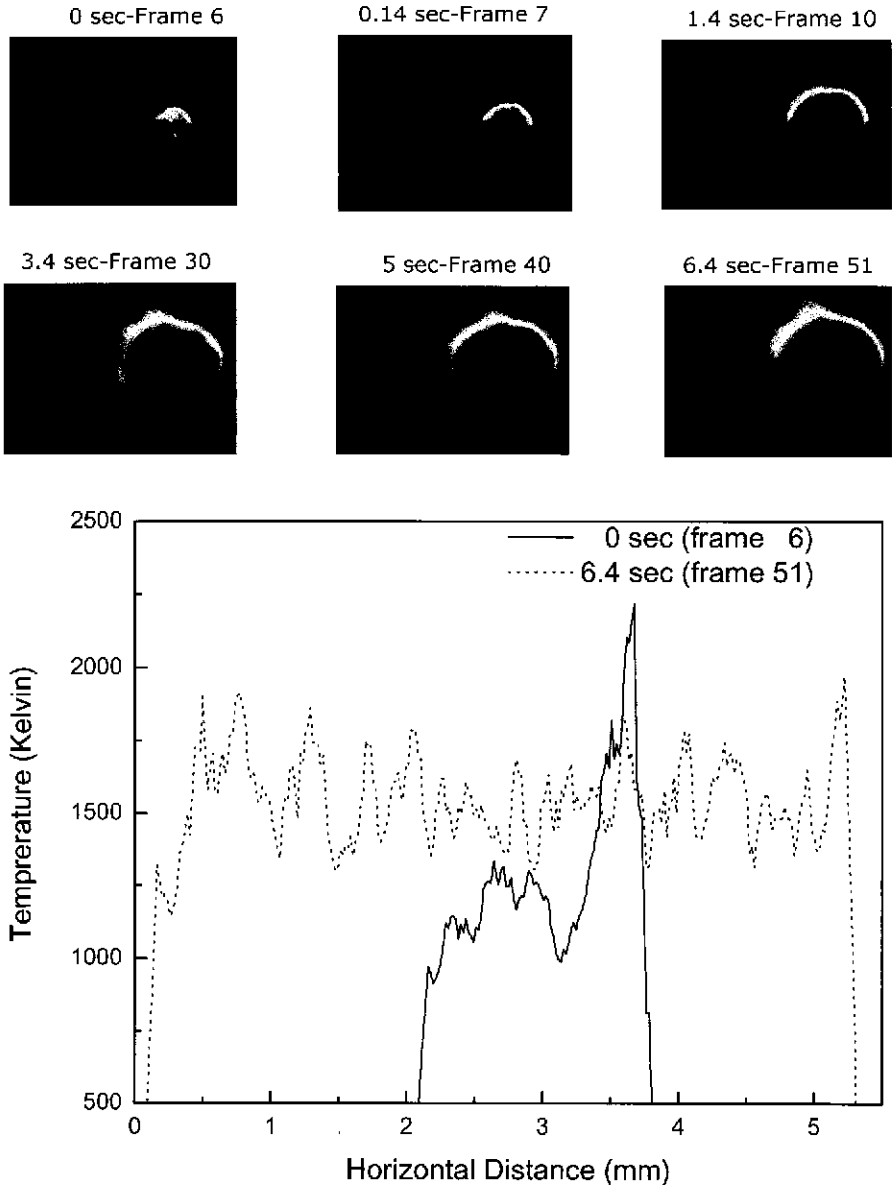

Fig. 3. Temperature profiles on the front surface of a 1-in.-diameter, 0.0625-in.-thick stainless steel disk illuminated by a 300-W, 18.7-MHz FEL beam focused to 10 kW/cm^2 for 10 s.

For example, spatially averaged heated spot temperatures calculated from emission spectra show that 1-in.-diameter samples irradiated with 300 W reached the melting temperature of steel. But smaller-diameter samples thermally isolated from their surroundings reached higher spatially averaged temperatures under similar irradiation conditions. One example of this is shown in Fig. 4, where we compare temperatures reached by a standard 1-in.-diameter

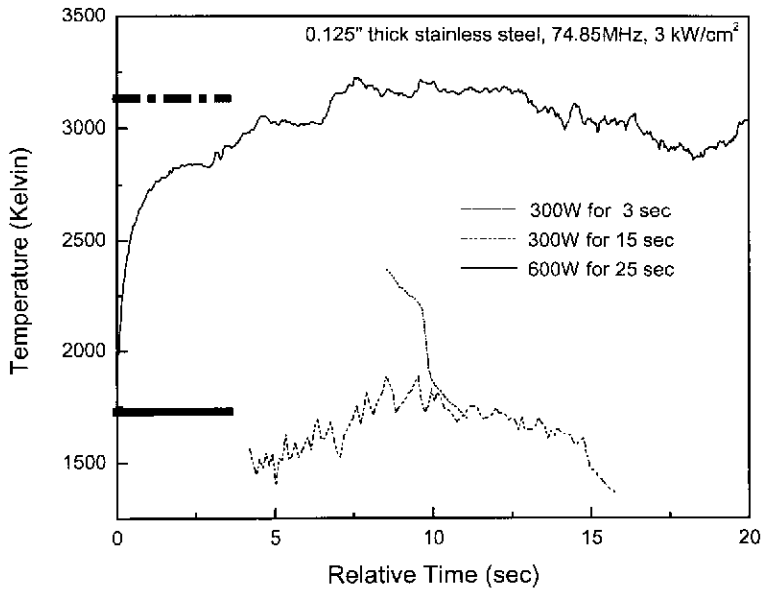

Fig. 4. Spatially averaged front surface emission temperatures of three 0.125-in.-thick stainless steel samples exposed to a 74.85-MHz FEL pulse train focused to produce 3 kW/cm^2 on the sample surface. The sample exposed at 300 W for 15 s had a 1-in. diameter. Another sample was exposed at the same power for 3 s, 1/5th the time, and yet it reached a temperature approximately 30% higher then the melting temperature of steel. The diameter of this sample was 0.25 in. The sample exposed at 600 W had a diameter of 1 in. and reached a temperature equivalent to the boiling temperature of iron, the main constituent of stainless steel. Horizontal lines represent the locations of melting and boiling regions of steel.

steel sample to a special case of a 0.25-in. (0.125 in. thick)-diameter sample. Both samples were irradiated at 300 W, with a 74.85-MHz repetition rate and a focal spot designed to give 3 kW/cm^2. Even though the smaller-diameter sample was irradiated for only 1/5th the time of the larger-diameter sample, it reached an average temperature of at least 2,200 K, 30% higher than the temperature of the 1-in.-diameter sample. The 30% or greater temperature difference is a measure of the effect that thermal conduction has on the irradiation of large-diameter samples.

Another example, also in Fig. 4, compares the spatially averaged temperature of a standard 1-in.-diameter (0.125 in. thick) stainless steel sample irradiated with 600 W instead of 300 W. Its temperature rose to the boiling temperature of iron, ~3,000 K. It was not obvious from a visual inspection of the samples which was heated to a melting and which to a boiling temperature. One may conclude that the energy used to boil the steel is wasted since melting the steel would be good enough to damage the sample.

Besides measuring the emission temperature profiles on the front, laser-illuminated, side of the target it is also possible to measure temperature profiles on the back of the target and to watch the target melt and burn through. This type of measurement, when temporally synchronized to the same diagnostic on the front of the target, can be used to measure burn-through times and heat conduction. Without synchronization, the dimension of the heated spot is a function of target thickness, and a measurement of what happens to the melted

material at the target back (e.g., resolidification causing hole closing) is possible. Camera synchronization necessary to perform burn-through measurements has not been done in this experiment, but data at the target rear independent of data at the target front have been taken. Figure 5 shows such data on stainless steel irradiated with a 650-W, 74.85-MHz FEL focused to produce 0.5 kW/cm^2. The data show a flat temperature profile at the rear of the target, initially in a small spot, the spot growing in size, until eventually, at 5.7 s, a hole is burned through the steel. The melted material from within the hole drips down the rear side of the target, eventually forming two hot nodules that resolidify and then disappear from the image. The shapes of the hole as well as the resolidified nodules are comparable to what is observed on the exposed samples after the experiment.

Stainless steel Q^* for samples exposed at 1 kW/cm^2 were 12 kJ/g, much higher than the 4.4 kJ/g typically measured at similar irradiances and wavelengths on lasers other than the FEL.[12] The most likely explanation for this is that the FEL, having an output of $\sim$1 kW, had to be focused to small spot sizes to produce the stated irradiance and lateral thermal conduction played a significant role. Q^* of 4.4 kJ/g were measured with 10–100 kW continuous wave (CW) lasers focused to larger spots so that thermal conduction played a smaller role.

3.2. Aluminum

Experience with infrared CW lasers at less than 50 kW/cm^2 indicates that painted aluminum samples damage more severely than unpainted ones.[11] This is because unpainted samples reflect much of the incident laser energy, having only 3–7% absorption at 3 μm, thereby experiencing a lower thermal load than they would experience if most of the laser energy was absorbed. A less-than-50-kW/cm^2, infrared CW laser, when irradiating a painted metal surface, first cooks the volatile gases out of the paint, leaving a paint residue, which is highly absorbing (50 to 80%). Carbon char and pigment in the paint absorb the laser energy, which is then conducted to the underlying aluminum, causing the aluminum to melt. The paint residue adheres tenaciously to the metal and is not removed by high-velocity airflow. The paint residue in aluminum affects molten metal even in the absence of strong airflow; it seems to be incorporated in the molten layer providing the surface tension, which prevents the metal from flowing out of the target. At more than 50 kW/cm^2 the paint is more cleanly removed and painted and unpainted aluminum have similar penetration times.

A conventional, pulsed, non-FEL meant for directed energy lethality typically has pulse durations from hundreds of nanoseconds to many microseconds and a 100–1,000-Hz repetition rate and delivers on the order of joules per pulse. Because of the low repetition rate each pulse must itself cause significant damage and thus is focused to joules per square centimeter per pulse and peak irradiances of order 10^2–10^5 kW/cm^2. At such irradiance levels, a single laser pulse or a few pulses cleanly remove all the paint from a sample surface, leaving bare metal behind. Thus, subsequent pulses suffer from the high reflectivity the first few pulses created.

What happens when painted aluminum is exposed to an FEL is not a priori clear. An FEL's pulse duration is of order of a picosecond, its repetition rate is tens of megahertz, it delivers fractions of a millijoule per pulse, and it is focused on the sample surface to millijoules per square centimeter per pulse. At less than 50-kW/cm^2 average irradiance, the FEL's peak irradiance can be hundreds of kilowatts per square centimeter. An FEL pulse used in a directed energy weapon configuration, therefore, can have average power characteristics of a low-power CW laser—and not remove paint efficiently—and peak power characteristics of a conventional pulsed laser—which cleans paint effectively. Which is it?

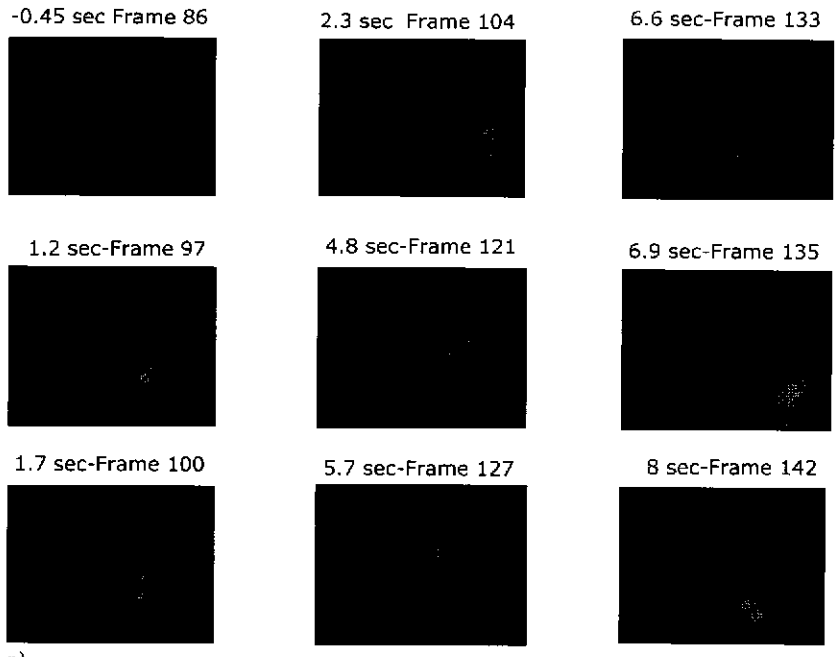

a)

b)

Fig. 5. a) Emission temperature at the rear surface of a stainless steel target exposed by a 74.85-MHz, 650-W FEL pulse train focused to produce 0.5 kW/cm^2 on the target surface. The hot-spot diameter at the rear grows from an initial 1.7 mm to 8 mm at the moment of burn through. The asymmetry in the hot spot after burn through is caused by molten material dripping down the target rear. b) The sample after exposure. The scale shown has 1-mm divisions.

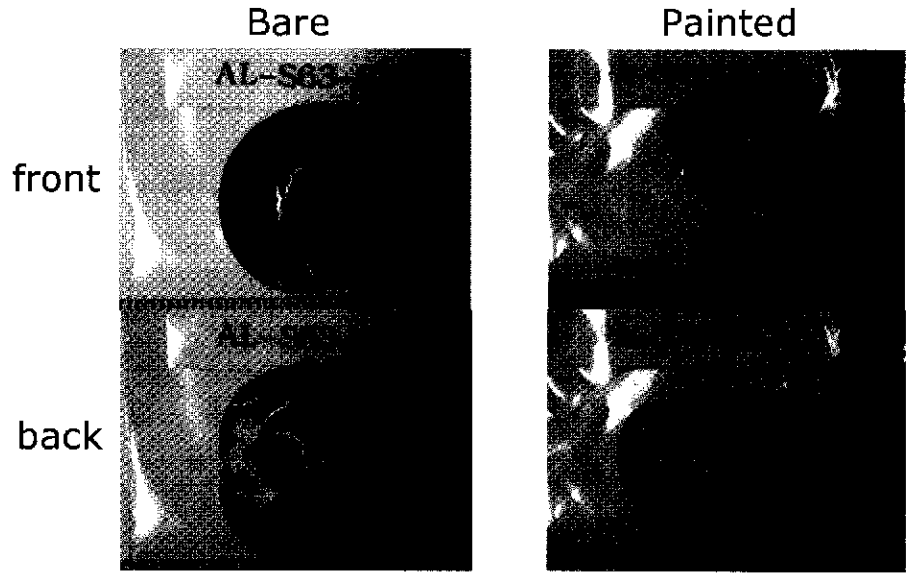

Fig. 6. Damage to aluminum samples AL-S63-S2 (unpainted) and PA-S72-SL1 (painted). Both samples were illuminated with a 600-W, 74.85-MHz laser beam focused to an average irradiance of 10 kW/cm^2. The samples were irradiated for 20 and 15 s for bare and painted, respectively.

It appears that the FEL behaves like a low-power CW laser and does not remove paint efficiently. To show this, experiments using 10-kW/cm^2 average irradiance and 10^5-kW/cm^2 peak irradiance were performed on unpainted aluminum (6061 alloy) samples and on the same aluminum samples painted with the current Navy aircraft paint process using a chromate conversion coating, primer, and gray topcoat.[§§] Postshot examination of the samples indicates that paint char remains on the aluminum, causing enhanced absorption and more serious damage. This can be seen in a postirradiation examination of painted and unpainted aluminum samples such as the ones shown in Fig. 6. Time-resolved temperature profile measurements likewise show that the painted target reached a temperature of ~1,800 K while the unpainted target reached a 20% lower temperature of ~1,500 K. Both temperatures are higher than the melting temperature of aluminum, which is about 1,000 K, but lower than the boiling temperature of about 2,800 K (Fig. 7). The painted aluminum sample (see Fig. 6) was severely damaged, and much of it was not recovered after the test. Some of the molten aluminum that remained coalesced under surface tension in the rearward region where there was little or no airflow. In the case of the bare aluminum the heating was slower. A hole probably formed in the sample but then filled as the melt slumped on the back under gravity. About half of the sample was in the flowing melt stage. The surface was heavily oxidized, as shown by the shiny unoxidized aluminum revealed in the cooling cracks. The rear shows an area seemingly spray-painted white. This is probably vaporized

[§§]The samples were cleaned, degreased, deoxidized, and chromate (Alodine 1200S) pretreated, primed with MIL-PRF-85582C, Type II Class C2, and topcoated with MIL-PRF-85285C, Type I, Gray color 36375. The total dry film thickness is on the order of 0.002 in.

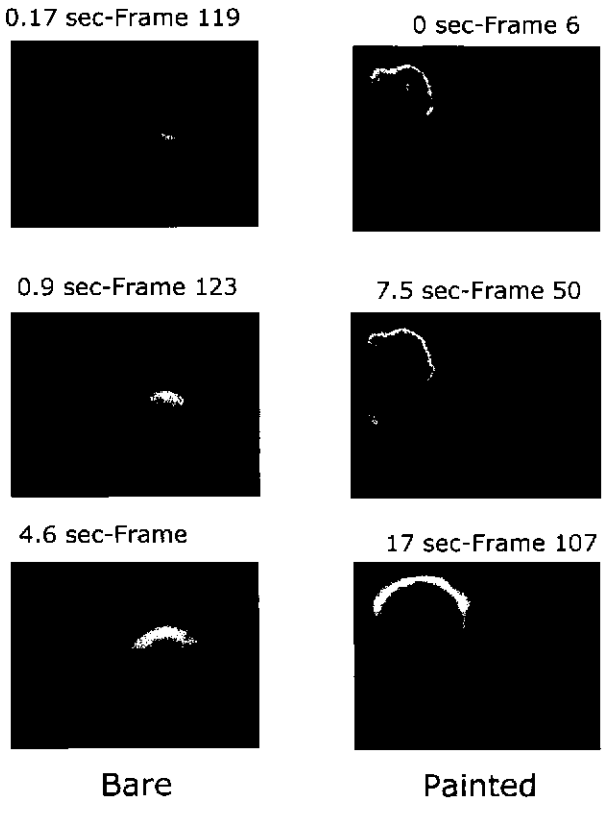

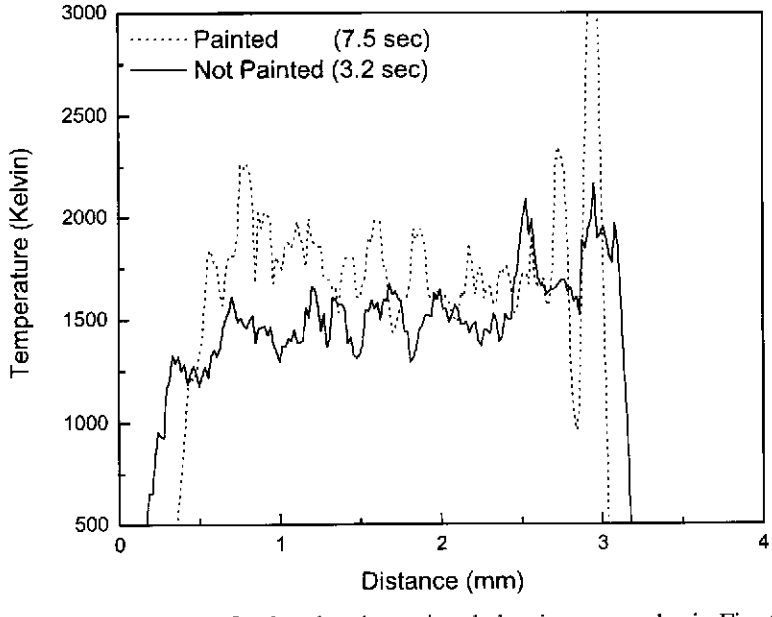

Fig. 7. Temperatures of painted and unpainted aluminum samples in Fig. 6.

and redeposited MgO, as magnesium is present in the alloy at the 1% level and readily oxidizes. In later experiments, when the irradiation time was considerably reduced, the bare aluminum appeared to be untouched, while the painted sample showed considerable melting damage. Thus, at the 10-kW/cm^2 and lower level, the FEL behaves as a CW device.

Q^* on bare aluminum samples for samples exposed at 1 kW/cm^2 were 27 kJ/g, compared to 11.5 kJ/g typically measured at similar irradiances and wavelengths on lasers other than the FEL. The explanation for the discrepancy is the same as the one given earlier for the steel samples.

3.3. Organic glass composite

A glass cloth held together by an organic resin, a type used in radomes, was tested. The probable damage sequence for this material, at least when irradiated slowly, is as follows.[4] First, energy is absorbed by the organic resin within target. The resin vaporizes, producing carbonized char that further absorbs and heats. At temperatures of 573–750 K the resin cooks out from between the fibers of the glass-cloth weave. Forty percent of the mass in the target is lost between the temperatures of 573 and 673 K, and another 15% between 673 and 750 K. The carbon char itself sublimes at 3640 K.[¶¶] The carbon is hotter than the supporting glass fiber can tolerate, and so the fiber melts as the carbon on its surface sublimes.

Figure 8a shows a frame from a time sequence of measured emission temperatures for this composite when irradiated by a 1,000-W, 74.85-MHz FEL pulse train focused to 10 kW/cm^2. The 1-mm-weave of the glass cloth of the target and the organic resin in between the glass fibers are clearly visible in the photograph, and from the temperatures of each one can infer the process occurring at the time the image was taken. For example, the black regions on the image designate temperatures lower than about 700 K, indicating the locations of resin cook off. Dark gray regions are ~950 K and light gray ~2,500 K. White regions, which register at ~4,000 K, are regions where the carbonized char is sublimating. The spatially averaged temperature of the target measured with the spectrometer is 2,900 K. For comparison, photographed images of the damaged target are shown in Fig. 8b.

A time sequence of the emission temperatures of samples exposed at a lower irradiance of 0.5 kW/cm^2 is shown in Fig. 8c. The sample in this case was exposed by an FEL run at 650 W and 74.85 MHz. The time sequence shows the evolution of temperature through to hole burning and the separation of individual strands of glass from the bulk of the target. At about 10.4 s after the appearance of the first image the average temperature on the target surface is ~1,750 K.

3.4. Pyroceram and SCFS

A Pyroceram radomelike material was tested under illumination conditions identical to certain illuminations of the organic glass composite. The sample showed melting occurring in the illuminated region and, interestingly, cracks propagating in opposite directions from within the melted region. Spatially averaged but time-resolved temperature measurements indicated that the front surface was about 2,800 K, significantly higher than the Pyroceram melting temperature of 1,620 K or even the Pyroceram vaporization temperature of 2,200 K. This temperature was also similar to the front-surface temperature measured on the glass

[¶¶] The char (carbon) sublimes before it melts; the melting temperature of carbon is about 3,820 K.

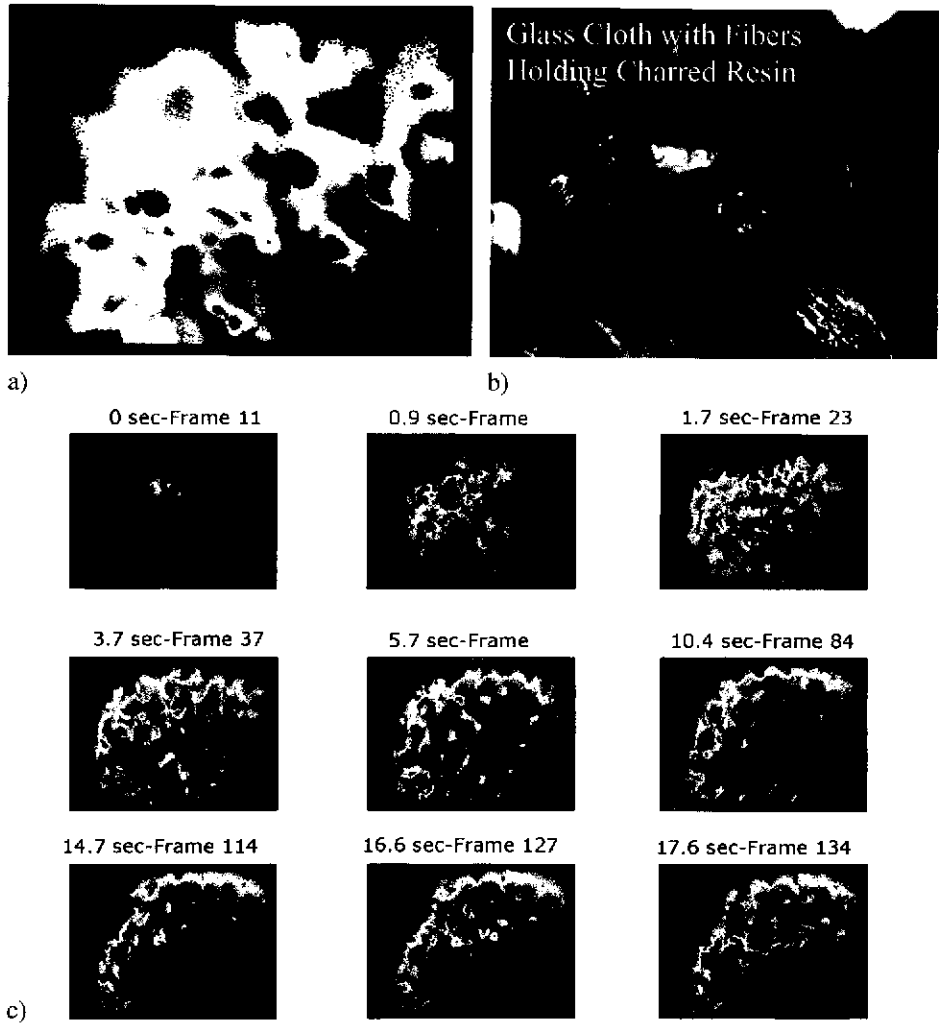

Fig. 8. a) Temperature profile of an organic cloth composite when irradiated by a 1,000-W, 74.85-MHz FEL pulse train focused to 10 kW/cm^2. Black regions on the image signify temperatures lower than about 700 K, indicating the locations of resin cook off. Dark gray regions are ~950 K and light gray about ~2,500 K. White regions, which register at ~4,000 K, are regions where the carbonized resin (char) is subliming. b) Optical image of the same target after the shot showing remnants of the glass cloth held together by carbonized char. Glass fibers in both images are 1 mm apart, giving the approximate scale in both images. c) Time sequence of the emission temperatures of an organic glass composite exposed by an FEL run at 650 W and 74.85 MHz and focused to 0.5 kW/cm^2.

composite under the same conditions (Fig. 9). The temperature, however, was lower than that of identically illuminated slip-cast fused silica (SCFS) SiO_2 radomelike material on which we measured spatially averaged temperatures of 4,100 K ±5%. As is the case with Pyroceram, these temperatures are much higher than either the melting (1,980 K) or vaporization (2,300 K) temperatures of SCFS. Unlike Pyroceram, SCFS showed no signs of

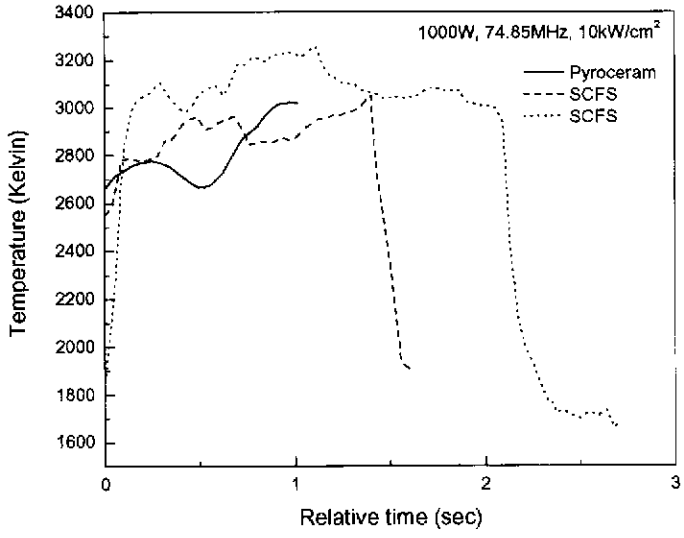

a)

b)

Fig. 9. a) Time-resolved temperatures of a Pyroceram target compared to those from an organic cloth composite irradiated at 1000 W, 74.85 MHz, and 10 kW/cm^2. b) Images of a Pyroceram sample (left) and a SCFS sample (right) after irradiation. Note damage in the form of cracks on the Pyroceram and droplets of solidified SiO_2 on the SCFS. (The scale divisions in the photograph are millimeters.) The formation of these droplets while they are still in the liquid state was measured with the four-frame imager.

cracking or damage far outside the focal region. Within the focal region solidified liquid SiO_2 droplets arranged in a pentagonal structure (Fig. 9) were observed. A time sequence taken by the four-frame camera captured these droplets in the process of formation, while they were still in a liquid state. The behavior of the liquid droplets seen on the four-frame camera is reminiscent of Benard convection cells observed, for example, in cooking liquid.

Q* measured on SCFS at 1 kW/cm^2 were unusually high, at 550 kJ/g, compared to 12 kJ/g measured on other non-FELs. Thermal diffusion from small spot sizes is an unlikely

explanation for this large discrepancy since thermal conductivity for nonmetallic samples is much smaller than for metallic samples such as aluminum and steel. (Furthermore, on other types of nonmetallic samples irradiated at 1 kJ/cm^2, such as Plexiglass, Q^* of 3 kJ/g were the same for this FEL and non-FELs.) Rather, the explanation here is that in the absence of strong airflow molten SCFS resolidifies on the sample surface, as shown in Fig. 9, causing erroneous inferences of Q^* from measurements of removed mass.

4. Summary

Samples of various materials, such as stainless steel, painted and unpainted aluminum, fused silica, and fiberglass, were irradiated by a train of picosecond-duration pulses from a FEL at irradiances of 0.5–10 kW/cm^2. In situ and time- and space-resolved diagnostics that measure emission temperature were fielded on the experiment. In one diagnostic, images of light emitted from the laser-irradiated heated side of the samples were optically split into four components. Each image component was passed through a different narrow band interference filter, and then the filtered images were recorded by a CCD video camera. Appropriate software was used to convert the images into temperature profiles, and movies of the temporal evolution of the temperature were produced. Heating and cooling of the samples, hole burning, and flow of liquid matter were observed. Breakup of fibers was recorded in fiberglass composite samples. A similar diagnostic placed to observe the rear side of the sample measured heating of the sample rear and details of the burn through. Light emission from the focal region was also coupled into a time-resolved spectrometer that recorded visible lines and continuum for the target surface. Black-body fits to the continuum were converted into movies of the samples' spatially integrated front-surface temperature.

Surprisingly, the measurements showed that temperature profiles on the laser-irradiated side of the target were flat even though the targets were irradiated by a Gaussian-like laser profile. This is probably due to the surface temperature becoming clamped at the melting temperature of the sample and shows that uniform temperature results can be obtained even with nonuniform beams. Around the edges of some samples, temperatures close to boiling temperatures of the materials were measured. At some laser powers most emission from the sample was consistent with a boiling temperature. Temperature rise times of the samples varied depending on details of the experiment, such as laser powers, sample composition, exposure duration, and sample dimensions.

Temperature profiles of fiberglass composite samples exhibited a range of temperatures indicative of different processes occurring in different parts of the composite: Regions of resin cook off, sublimation of carbonized char, and the decomposition of the fiber cloth were measured. Flow of liquid material on the surfaces of fused silica samples was also observed.

Q^* measurements on metal and SCFS samples were much higher on this FEL than Q^* measured on other lasers under similar irradiance conditions. The likely reason for this is the small spot sizes used in these experiments and the lack of strong airflow over the sample surface. These shortcomings will be corrected in future experiments when the FEL is upgraded to 10 kW and a well characterized airflow nozzle is constructed.

5. Acknowledgments

We thank Maj. Franz Gayl (Ret.), Richard Gullickson, and Cmdr. Roger McGinnis for their support. We are also grateful to the staff at the Jefferson Laboratory whose professional

and dedicated support made these experiments possible. This work was supported by the High Energy Laser Joint Technology Office (HEL-JTO).

References

[1]*Aerospace Structural Metals Handbook*, AFML-TR-68-115, Code 1303, p. 1 (1972).

[2]Siggins, T., C. Bohn, L. Merminga, J. Preble, F. Dylla, G. Biallas, D. Douglas, J. Fugitt, K. Jordan, G. Krafft, G. Neil, B. Yunn, R. Walker, S. Benson, and M. Shinn, "A Kilowatt Average Power Laser for Sub-Picosecond Materials Processing," Thomas Jefferson Laboratory, Report JLAB-ACC-99-18 (1999).

[3]Chaney, J.F. (ed.), *Thermophysical Properties Research Literature Retrieval Guide, 1900-1980*, Vol. 1–7, IFI/Plenum (1982).

[4]Cozzens, R., R. Wenzel, J. Cook, C. Lloyd, S. Jensen, and T. Schriempf, *Laser Induced Char Effects on Missile Radomes*, 5th National Meeting, Directed Energy Professional Society, Monterey, CA, Nov. 2002; the degradation sequence was measured using relatively slow heating. Rapid heating with a pulsed laser may, possibly, give somewhat different results.

[5]*CRC Handbook of Materials Science, Vol. 1: General Properties*, CRC Press, Boca Raton, FL, p. 24 (1974).

[6]Grun, J., C.K. Manka, R. Fischer, R. Wenzel, R. Cozzens, and M. Shinn, "In-Situ Measurements of Temperature Profiles and Plume Formation at the Surfaces of Samples Irradiated by a Picosecond Laser Pulse Train," NRL Memorandum Report NRL/MR/6790—03-8656 (2003).

[7]Hopkins, M.F., Proc. SPIE **2599**, 294 (1995).

[8]Palik, E.D., *Handbook of Optical Constant of Solids*, Academic Press (1985).

[9]Rutgers, G.A.W., and J.C. Devos, *Relation Between Brightness Temperature, True Temperature, and Color Temperature of Tungsten*, Physica XX, pp. 715–720 (1954).

[10]Stair, R., R.G. Johnston, and E.W. Halbach, J. Res. Natl. Bureau Stand.–Phys. Chem. **64**A(4) 291 (1960).

[11]Wenzel, R. F., "Pulsed Laser Lethality Assessment," Naval Research Laboratory Memorandum NRL/MR/6330—02-8619 (2002).

[12]Wenzel, R., Private Communications from Multiple Sources (2003).

The Authors

Dr. Robert F. Cozzens received a B.S. degree in Chemistry in 1963 and a Ph.D. in Physical Chemistry in 1966 from the University of Virginia. He is a Professor of Chemistry at George Mason University in Fairfax, VA, and a Senior Research Scientist (Intermittent) at the Naval Research Laboratory in Washington, DC. Dr. Cozzens has been involved for 25 years in the interaction of laser radiation with materials, including polymeric composites, metals, coatings, ceramics, and human eyes, and has published and presented numerous research papers. He is a member of the American Chemical Society (ACS), Chemical Society of Washington (CSW), Directed Energy Professional Society (DEPS), and Materials Research Society (MRS). He has held several elected offices within the ACS and CSW.

Dr. Richard Fischer received his B.S., M.S., and Ph.D. degrees in Electrical Engineering from the University of Maryland, College Park, in 1984, 1986, and 1993, respectively. He has been a researcher in the Plasma Physics Division at the Naval Research Laboratory since 1988. His recent research has concentrated on novel radiation sources and the interaction of intense lasers with electron beams, semiconductors, and plasmas. This includes the laser synchrotron source experiment, athermal annealing of semiconductors, and the development of gyrotrons, quasioptical gyrotrons, and quasioptical gyroklystrons. Dr. Fischer is a member of IEEE and APS.

Dr. Jacob Grun received his Ph.D. in Physics from the University of Maryland in College Park. After receiving his Ph.D. Dr. Grun joined the Naval Research Laboratory, where he performed research in inertial confinement fusion, x-ray and laser testing of military components, laboratory simulations of nuclear explosions, astrophysical phenomena,

Naval hydrodynamics, and laser matter interactions. Dr. Grun is currently the head of the Laser Experiments Section in the Beam Physics Branch. He is a fellow of the American Physical Society and a member of the Materials Research Society and the Directed Energy Professional Society.

Dr. Michelle Shinn, FEL Optics Group Leader, has been at Jefferson Lab since 1995. From 1996 to 1999, she led the design, procurement, and installation activities for the IR Demo free electron laser (FEL) optical cavity, transport, and diagnostics, and since 1999 she has performed the same duties on the Upgrade FEL projects. She actively collaborates with a number of teams that use the FEL and, in particular, has been pursuing her own research on ablation of materials and laser-induced damage of optical components. Before coming to Jefferson Lab, she was a physicist in the Laser Division at Lawrence Livermore National Lab (1984–1990) and Associate Professor of Physics at Bryn Mawr College (1990–1995).